Triple probe interrogation of spokes in a HiPIMS discharge

F. Lockwood Estrin[1], S. Karkari[2] and J. W. Bradley[1*]

1. Department of Electrical Engineering and Electronics, University of Liverpool, Brownlow Hill, Liverpool, L69 3GJ, UK

2. HBNI, Institute for Plasma Research, Bhat Gandhinagar, Gujarat, 382428, India

*Author for correspondence: j.w.bradley@liv.ac.uk

Abstract

Using a triple probe situated above the racetrack and inside the magnetic trap of a magnetron, rotating spokes-like structures have been clearly identified in a single HiPIMS pulse as periodic modulations in the electron temperature T_e, electron density n_e, ion saturation current I_{isat} , floating potential V_f and plasma potential V_p. The spokes rotate in the E x B direction with a velocity of ~ 8.8 km/s.

Defining the spoke shape from the footprint of ion current they deliver to flush mounted probes embedded in the target, each spoke can be characterised by a dense but cool leading edge (n_e ~ 2.0 x 10^{19} m^{-3}, T_e ~ 2.1 eV) and relatively hotter but more rarefied trailing edge (n_e ~ 1 x 10^{19} m^{-3}, T_e ~ 3.9 eV). Measurements of V_p show a potential hump towards the rear of spoke, separated from regions of highest density, with plasma potentials up to 8 V more positive than the inter-spoke regions. Azimuthal electric fields of ~1kV/m associated with these structures are calculated.

Transforming the triple probe time-traces to functions of azimuthal angle θ and assuming a Gaussian radial profile for the plasma parameters, 2D spatial maps of n_e, T_e , and V_p have been constructed as well as the target ion current density J_p from the embedded probes. The phase relationship between T_e, V_p and n_e can be clearly seen using this representation with n_e leading T_e and V_p with a phase shift between them of ~ 50^o. Regions of maximum ion current to the target delivered by individual spokes coincide with the overlap of regions of high n_e and T_e measured above the target at a height of 15 mm. Ions created at elevated positions

above the target in the observed dense region will take several micro-seconds to reach the target so contributing the target ion current in following spokes.

1. Introduction

As a relatively new physical vapour deposition technique, high power impulse magnetron sputtering (HiPIMS) has the potential to deliver engineering quality thin films and coatings [1], characterised by deposition fluxes composed of a large proportion of ionized sputtered metals (up to 90 % in some cases) [2]. This is achieved through low duty pulsing (a few %) but with high peak target power densities, up to 10 kW cm^{-2}, giving rise to dense plasmas with high ionisation states of the sputtered material [3].

These pulsed magnetized plasmas, with typical on and off-times of 10's and 1000's of μs respectively, are highly dynamical in nature with spatially and temporally varying electron densities n_e and temperatures T_e. The former n_e can vary 10^{19} m^{-3} near the target in the on-time [1] to below 10^{15} m^{-3} in the off-time, with T_e (of beam like electrons) peaking close to 100 eV in an initial on-time burst and falling to 0.5 eV in the afterglow [4]. As with all forms of magnetron sputtering, the structure of plasma is largely determined by the looped magnetic topology which gives rise to mutually perpendicular electric and magnetic fields above the region of maximum target sputtering [5]. This region, were magnetic field lines intercept the target twice, is known as the magnetic trap, and is characterised by a substantial closed loop E x B (Hall) electron drift current [6].

One phenomenon of current interest to physicists and technologists studying HiPIMS is plasma self-organization. Coherent plasma structures, often called spokes, can be observed to sit above the target and circulate at speeds of several kms^{-1} around the Hall drift channel (as discussed in reference [7]). They rotate ostensibly in the E x B direction, however sometimes in the counter direction, particularly at low powers [8]. Since the first report of spokes in HiPIMS in 2011 [9], subsequent studies have revealed that spokes are common to all magnetrons (not just HiPIMS), for instance in magnetrons operating in DC [8], [10], [11]. The pattern of spokes can broadly be placed in three regimes: Coherent (fixed frequency and mode number), chaotic (random timings between spokes) or non-existent (either quiescent

conditions or one unified spoke). The observable spoke regime depends mainly on the working pressure and the instantaneous discharge power density [12], [13]. In some cases, particularly in HiPIMS, coherent patterns of spokes have been seen to evolve through merging and splitting events [14], [15] during a pulse. Therefore, in general there is no precise pulse-to-pulse repeatability in the timing of spokes (their azimuthal phase) or their precise shape.

Spokes are not only seen in magnetron devices but also in other discharges characterised by strong closed-path E x B drifts, including Hall thrusters [16], and homo-polar plasmas [17]. However, spokes may be of particular important in HiPIMS, as they have been linked to the generation of anomalously high ion energies [18], [19], with ramifications for thin film growth. It is argued that they may also eject ions in radial directions, so reducing the coating flux towards the substrate [20].

To observe spokes and to understand their structure and behaviour a number of diagnostic techniques have been used on HiPIMS plasmas. Non-perturbing optical techniques have been employed which allow a full view of the cathode and effectively a “photograph” of the spokes: these include fast 2-D ICCD images of the broadband emission [13], [15], [21], spectrally filtered 2-D images [22], a photo-multiplier tube (PMT) view via optical slits [23] and laser-induced fluorescence (LIF) imaging [22]. Spokes have also been identified optically using single [24] and multiple optical fibres [25]. Streak cameras have been used to view spokes side-on so revealing the existence flares (interpreted as electron jets) which emanate from the top of the spoke travelling upwards in columns [21], [26]. Other non-perturbing studies to detect the presence of spokes include monitoring of the changes in the external discharge current-voltage characteristics [13], [27], the use remotely situation mass energy analysers to detect spoke-generated high energy ions [18], [28], including measurements made at right angles to the target [19] and angularly resolved measurements [20]. In addition, non-perturbing flush mounted embedded probes in the target have been developed to measure the current individual spokes deliver to the target [12], [15]. Although invaluable in providing information of spoke structure, many of the optical imaging techniques do not yield quantitative information about the spoke parameters. Some of these techniques have been combined however to good effect such, as the use of fast 2D ICCD imaging and target probes [15].

One of the workhorse diagnostic tools used on low-pressure plasma is the electrical (Langmuir) probe. Although perturbing to the plasma, they can yield local values of the plasma electron density (n_e), electron temperature T_e, floating potential V_f and plasma potential V_p and in some cases the electron velocity distribution function $f_e(v)$. Electrical probes have used to detect the presence of spokes in a number of recent HiPIMS studies, including the use of single cylindrical Langmuir probes to identify spokes in the floating potential V_f [29] and the ion saturation current I_{isat} [30]. An array of radially separated planar (single) probes placed around the target was used to detect variations in V_f [14]. Single planar probes were used to detect changes in I_{isat} and V_f, fluctuations [23] and also in the electron saturation I_{esat} [19]. Emissive probes have deployed to observe the time-modulation in the plasma potential V_p [21], and a double flat probes to observe, V_f and I_{isat} oscillations [31]. Other useful measurement techniques include the use of magnetic sensor probes to identify the presence of spokes and their effect on the magnetic topology [32]. An emissive probe and a single probe has been used in conjunction to determine with great effect the plasma potential V_p and electric field structure inside spokes in a low power DC magnetron [11].

Although fast (real time) measurements of I_{isat} and V_f are possible with a Langmuir probe, the lack of pulse-to-pulse repeatability in the timing and structure of spokes in HiPIMS discharges makes acquiring full probe characteristics over a number of periods problematic. This may be one reason why the plasma parameters (i.e. n_e and T_e) associated with spokes has yet to be determined. In addition, to avoid perturbation of the discharge, probes have been placed mostly at remote positions, outside the magnetic trap, where only the influence of spokes on the bulk plasma is detected rather than probing the spokes themselves.

To measure n_e and T_e within a single spoke using a Langmuir probe, would require a fast voltage sweep. With typical spoke velocities of ~10^4 ms^{-1} [7] and azimuthal extensions of a few centimetres (e.g. see [15]) full sweep and data collection frequencies of 100 kHz or faster would be needed to resolve detail with in a spoke. Such single probe systems have been employed to observe plasma parameter instabilities and fluctuations in fusion device edge regions [33] but are not routinely available in most HiPIMS laboratories.

One solution is to use a triple probe, which under certain assumptions can yield directly measurements of the basic plasma parameters (V_f, T_e and the ion saturation current I_{isat}) with

excellent time-resolution. A simple calculation using the I_{isat} and T_e time-traces can provide the electron density n_e. Similarly, T_e and V_f can be used to calculate the plasma potential V_p.

The triple technique was originally proposed by Chen and Sekiguchi in 1965 [34] and first tested on a magnetized diode air plasma discharge. Since then the diagnostic, which can provide sub-microsecond time-resolution, has been used extensively on a wide range of relatively dense plasmas from tokamak edge plasmas [35], to pulsed magnetrons [36] and HiPIMS plasmas [37]–[40]. Interesting in [40] it was reported that time-traces of n_e and T_e made on the centre line of the discharge showed coherent modulations in these parameters with periods of 20 - 50 μs, equivalent to frequencies of 50 - 20 kHz respectively. Although no explicit investigation of spokes was made in that study, these modulations are not inconsistent with typical spoke frequencies seen elsewhere. The fluctuations in T_e and n_e were close to being in anti-phase; however observations were not discussed in relation to spokes.

Here we use a triple probe to diagnose the plasma inside the magnetic trap, directly above the racetrack, namely in a region where we expect spokes to pass or at least have a significant effect on the plasma there. To do this, we must assume the electron energy distribution function (eedf) in the region of measurement is a Maxwellian distribution, with a characteristic temperature T_e. This assumption is largely supported by a body of experimental work undertaken on dc and pulsed-dc magnetrons which shows the eedf is usually well fitted by a Maxwellian in the vicinity of the cathode (inside the magnetic trap region) and by a bi-Maxwellian further away from it [41]–[43]. In dense HiPIMS plasmas ($n_e > 5 \times 10^{18}$ m^{-3}) with long on-times (> 10's of microseconds) there is sufficient time for the eedf's of electrons in the magnetic trap to reach a steady state configuration, as discussed by Gallian et al [44] in a kinetic modelling study of a HiPIMS plasma operating with an aluminium target. Energetic secondary electrons liberated from the cathode will Maxwellianize in that region, in a few 10's of nanoseconds. The predictions for the eedf in Ref [44] show that inside the magnetic trap, the vast majority of electrons do relax to form a cold Maxwellian distribution, however with a hot tail of electrons emerging for electron energies above ~30 eV. This energetic group, originating from the interaction of sheath-accelerated secondary electrons with heavy gas and metal species is four orders of magnitude smaller than the main group. At these low concentrations, such beam-like energetic electrons in the eedf will not affect a typical

Langmuir probe characteristic [45]. We are therefore confident that our assumption of a Maxwellian eefd in the dense plasma of the magnetic trap is a good one, and that any small non-Maxwellian character would be essentially undetectable in the triple probe analysis.

Here, the magnetron is operated in conditions known to produce coherent spokes [12] and measurements are taken over a single HiPIMS discharge pulse, in which the spoke mode number m changes smoothly from m = 5 to m = 3.

2. Experimental arrangement

2.1 The magnetron system and power supply

The magnetron used in this study was a circular unbalanced type, equipped with a 75 mm diameter niobium target of 5.53 mm thickness and purity 99.95%. It was situated at one end and facing the centre of an aluminium chamber of internal diameter 270 mm and length 300 mm. The basic experimental system is also described in reference [12] and is shown schematically in figure 1a.

The system was pumped down to a base pressure of 10^{-4} Pa using a turbo-molecular pump (Edwards EXT75DC) backed by a rotatory pump (Edwards E2E28). In operation, the system was back-filled with argon gas through a MKS 1179A mass flow controller at flow rates between 10 – 50 sccm to achieve chamber pressure from 0.33 - 1.7 Pa, measured using a capacitance manometer pressure gauge (MKS 628A).

An in-house built HiPIMS power supply [46] was used to deliver a 200 μs voltage pulse at a repetition rate of 1 Hz, with energy per pulse of 6.8 J. To allow operation at this low frequency, a DC simmer source was used, providing a DC voltage to the cathode of about -200 V.

The vacuum magnetic field strength in the region above the target was measured on the bench top using a GM07 Gauss-meter (Hirst Magnetics). The magnetic field configuration and position of the triple probe used in the study are shown in figure 3. The magnetic field strength at target surface at the centre of the racetrack (determined to be a radius of 21.5 ± 0.5 mm) was measured to be 498 G.

2.2 Embedded target probes

To determine the current delivered to the target by individual spokes as they rotate, a system of flush mounted probes was developed as described in detail in [12], [15]. The target probes consisted of three 2 mm wide and 35 mm long niobium strips (and of the same purity as the target). These were push-fitted into three corresponding radial slots of width 2.14 mm cut in the target to form a flush surface, with 10 mm of each probe protruding over the edge of the magnetron circumference. This was to allow ease of electrical connection. It was assumed that negligible ion current was drawn to this protruding region compared to that received over the target and therefore the effective area of probes was taken to be 2 mm x 25 mm = 50 mm^2. To electrically insulate the strip probes from the target the strips were covered on three sides by a polyimide tape of thickness of 0.07 ± 0.01 mm. This thickness defined the gap between the probe and the target. The three strip probes were separated azimuthally from each other by an angle $\theta = 25^o$, as shown in figure 1b.

To measure the current provided to the target by individual spokes as they pass over the strips, each strip was connected to the power supply as shown in figure 1c ensuring each maintained the same potential as the rest of the target. Their individual current contributions were measured using by a set of three Pearson current probes (Model 2877 with 1 V/A), with currents from strip probes 1 (- 25^o orientation) and 3 (+25^o orientation) being displayed on oscilloscope 1 (Tektronix DPO 4034) and the current from strip 2 (0^o orientation) displayed on oscilloscope 2 (Tektronix DPO 3034). The total discharge current I_d was measured using model 3972 (0.1V/A) Pearson current probe and the discharge voltage V_d measured with a voltage probe (Tektronix P5100). The values were displayed on oscilloscope 1. Both oscilloscopes were synchronized and triggered by a voltage signal from the HiPIMS power supply.

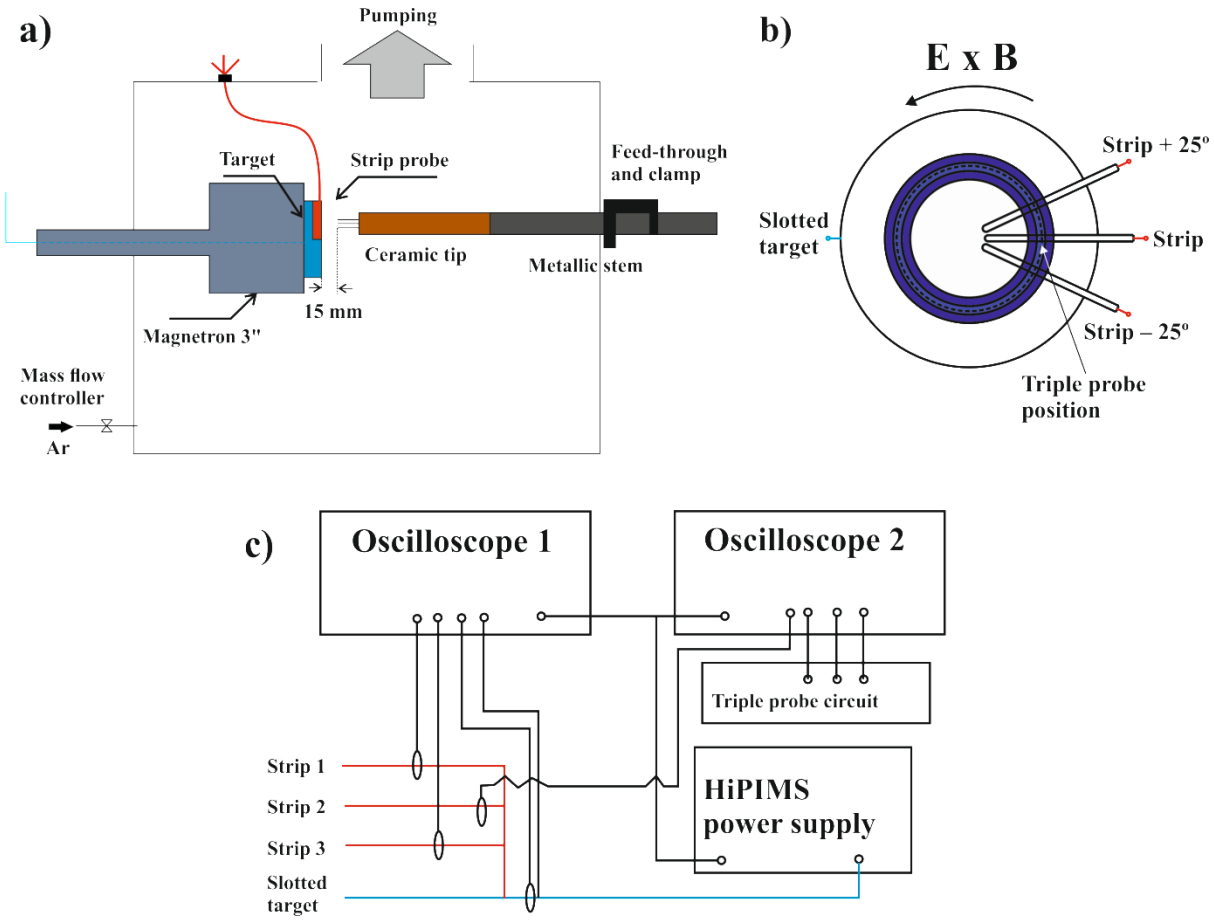

Figure 1. Schematic diagrams of a) the magnetron discharge and triple probe situated in the chamber, b) the strip probe and slotted target arrangement and c) the strip probe current and triple probe voltage measurement arrangement.

2.3 Triple probe theory

In the normal triple probe configuration three equal sized probe tips (shown as P_1, P_2, P_3 in figure 2) are used simultaneously to sample a small volume of plasma (or at least see nominally the same plasma). It is necessary that the tips are separated sufficiently so that the ion sheaths adjacent to their surfaces do not overlap. Typically triple probes are operated in the so called voltage mode, but can also be used in current mode [47]. Two of the probes (P_1 and P_3) are biased relative to each other (by voltage V_{13}) forming essentially a double probe configuration [48] with one of the probes (here P_3) biased well into ion saturation region (of a single probe characteristic). The remaining probe (P_2) is left to obtain the local floating

potential V_f, drawing no current. To ensure the current I_3 drawn to P_3 is in the ion saturation region, we must choose $V_{13} > kT_e/e$ (i.e. > the voltage equivalent of the electron temperature).

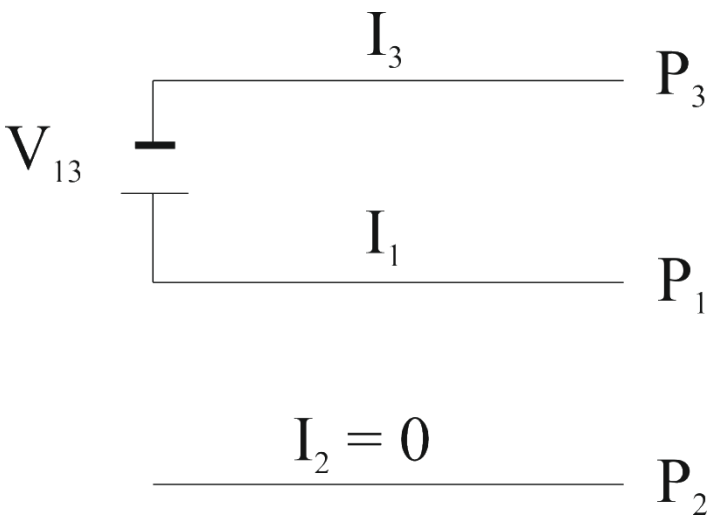

Figure 2. A schematic diagram of the triple probe arrangement for voltage mode analysis

Assuming a Maxwellian distribution of electron energies in the plasma with temperature T_e, the current I (V_b) drawn to a probe at bias V_b, in the transition region between ion and electron saturation regions ($V_b < V_p$), can be derived from the equations given in [48] to be;

$$I(V_b) = I_{isat}\ \left(1 - \exp\left(\frac{e(V_b - V_f)}{kT_e}\right)\right) \qquad (1)$$

where V_f is the floating potential and I_{isat} is ion saturation current. K is the Boltzmann constant and e the electronic charge. Given a thin, collisionless sheath with free-fall ions $I_{isat} = 0.61 e n_i A_{eff} (kT_e/ m_i)^{1/2}$, where n_i is the positive ion density, m_i is the ionic mass, e is the electronic charge and A_{eff} is the effective area of the probe [34].

Following an analysis in [34], the probe currents to the three tips (namely I_1, I_2 and I_3 expressed in the form stated in equation 1) can be readily combined to yield the relationship:

$$\frac{I_1 - I_2}{I_1 - I_3} = \frac{1 - \exp(-eV_{12}/kT_e)}{1 - \exp(-eV_{13}/kT_e)} \qquad (2)$$

Where $V_{12} = V_1 - V_2$ and $V_{13} = V_1 - V_3$. Current continuity gives, $- I_1 = I_3$ and the floating condition of probe P_2 ensures $I_2 = 0$. These conditions reduce the left hand side of equation 2 to ½. For a sufficiently large bias $V_{13} >> kT_e/e$ equation 2 becomes:

$$V_{12} = Log_e(2)kT_e/e \quad (3)$$

Inspection of equation 3 reveals that the electron temperature T_e can be obtained directly from the measurement of the difference between the floating potential V_2 (= V_f) of probe P_2 and the potential V_1 on probe P_1.

In the absence of negative ions, the ion density n_i and electron density n_e are assumed to be equal and can be found from measurement of the ion saturation current (as stated above), namely $n_e = I_{isat} / 0.61eA_{eff} (kT_e/ m_i)^{1/2}$. Following the analysis in [34] we have:

$$n_e = \frac{1}{0.61eA_{eff}\sqrt{kT_e/m_i}} \left[\frac{I_1}{exp\left[\frac{eV_{12}}{kT_e}\right] - 1} \right]$$

and in the limit $V_{13} >> kT_e/e$ we have that $eV_{12} /kT_e \sim Ln(2)$ yielding the simple form;

$$n_e = \frac{I_1}{0.61\, eA_{eff}\sqrt{kT_e/m_i}} \quad (4)$$

Voltages V_1, V_2, V_f and current I_1 can be captured and displayed on a digital oscilloscope, yielding after some simple manipulation time-resolved quantities of $n_e(t)$, $T_e(t)$ and $V_f(t)$ as well as an approximate value for the plasma potential $V_p(t)$ as described later in section 3.

2.4 The triple probe arrangement

The triple probe consisted of three tungsten tips of length 5 mm and diameter 0.08 mm with the tips arranged in straight line and attached to a ceramic stem, as represented in figure 1a. The tips were separated from each other by 1 mm. The triple probe was positioned directly above the central strip probe at a height of 15 mm above the target, with a line between the

tips oriented radially (parallel to the strip probe direction). At this position, it was assumed the probe would directly intercept the spokes or the region just above them, but not unduly perturb the discharge. In this configuration the probe tips intercepted the same radial magnetic field lines. The magnetic field strength at the end of the probe tips was 100 Gauss, with no more than a 20 G variation over the full length of the tips. At this position, the electron Larmor radius was estimated to be approximately $r_{Le} \sim 0.45$ mm, calculated using reference [49], assuming an electron temperature of $kT_e/e = 3.5$ eV. This length is of the order of the tip interspacing (d = 1 mm), but with the gyro-motion of electrons ostensibly parallel to the tips and not across them.

The extension of the ion sheaths adjacent to the probes is characterised by the electron Debye length λ_{De}. Assuming electron densities in the range $n_e = 10^{18}$ - 10^{19} m^{-3} (justified as shown is section 3) we have a range of λ_{De} = 14 μm to 4.5 μm respectively [49]. This is considerably less than d. At operating (argon) pressures of a few Pascal, the electron-neutral mean free path $\lambda_{e\text{-}mfp}$ ~ a few cm's and ion-neutral mean free path $\lambda_{i\text{-}mfp}$ ~ mm's [50], so we can assume the ion sheaths to be collisionless as well as the region between tips. Comparing these important scale lengths we have $\lambda_{De} < d < \lambda_{i\text{-}mfp}, \lambda_{e\text{-}mfp}$, necessary conditions for validity of the triple probe method [34].

The maximum dimension presented to the plasma by the entire triple probe tip arrangement and therefore the passing spokes is 2.26 mm (given by 2 x 1 mm interspacing, 3 x 0.08 mm tip thickness and 2 x 0.01 mm sheath extensions). This defines the radial spatial-resolution of the probe system. Azimuthally the spatial resolution is 0.1 mm. 2D images obtained using fast cameras, show spokes to have radial widths of about a 1 cm [15], [51], so we argue that the three tips simultaneously sample the same plasma region within a spoke (or at least the plasma directly above it). Spokes are observed generally to rotate as a solid body form.

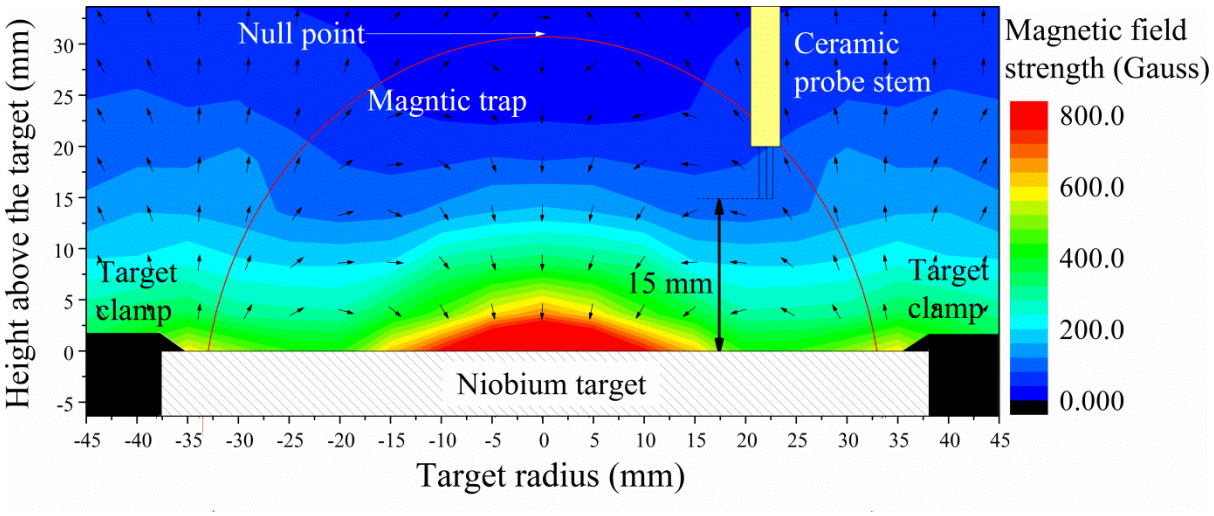

Figure 3. A 2D plot of the distribution of measured magnetic field strengths and their directions. The position of the triple probe inside the magnetic trap region is also shown. The probe tips are aligned with radial magnetic field lines and 15 mm from the target surface. The boundary enclosing the magnetic trap regions is shown as a solid red line.

The response time τ of the ion sheaths adjacent to the tips (and hence the fastest possible response time of the probe system) can be found from a calculation of the inverse ion plasma frequency (ω_{pi}^{-1}). Assuming electron densities as stated above, ω_{pi} lies between 2.1 x 10^8 s^{-1} and = 6.6 x10^8 s^{-1} [49] giving τ = ~ 4.7 – 1.5 ns. However, the time-resolution of the triple probe was set by the frequency response of the entire probe circuit. Ignoring the small sheath capacitance at the probe tips, the time-resolution τ_{res} was calculated from the product of the cable stray capacitance to ground C_{stray} and the dc sheath resistance R_s as described in Ref [52]. Using a Fluke digital multimeter, C_{stray} was measured to be 190 pf, for the combined 1.5 m long coaxial cable, probe assembly and feedthrough system up to the oscilloscope. The maximum sheath resistance R_s was estimated to be 42 Ω, calculated using $R_s = kT_e/eI_{isat}$ in accordance with Ref [52] with kT_e/e = 3.9 eV and I_{isat} = 0.09 A, taken from our measured data (as shown later in section 3). This gives a time-resolution $\tau_{res} \sim 10^{-8}$ s, sufficient to resolve spoke structures passing a fix point on time scales ~ 1 μs.

The triple probe tip potentials were measured using three Tektronix TPP0201 voltage probes (each with a 200 MHz bandwidth) connected to either oscilloscopes 1 (400 MHz bandwidth) or 2 (300 MHz bandwidth) via a resistance of 10 MΩ to the system unified ground. The probe current I_1, used to calculate n_e, was measured using a Tektronix TCP0030A (120 MHz

bandwidth) connected to oscilloscope 1. A floating voltage of 38 V was maintained between two of the probe tips (given as P_1 and P_3 in figure 2) using three lead acid batteries, each capable of providing 0.8 Amp hours.

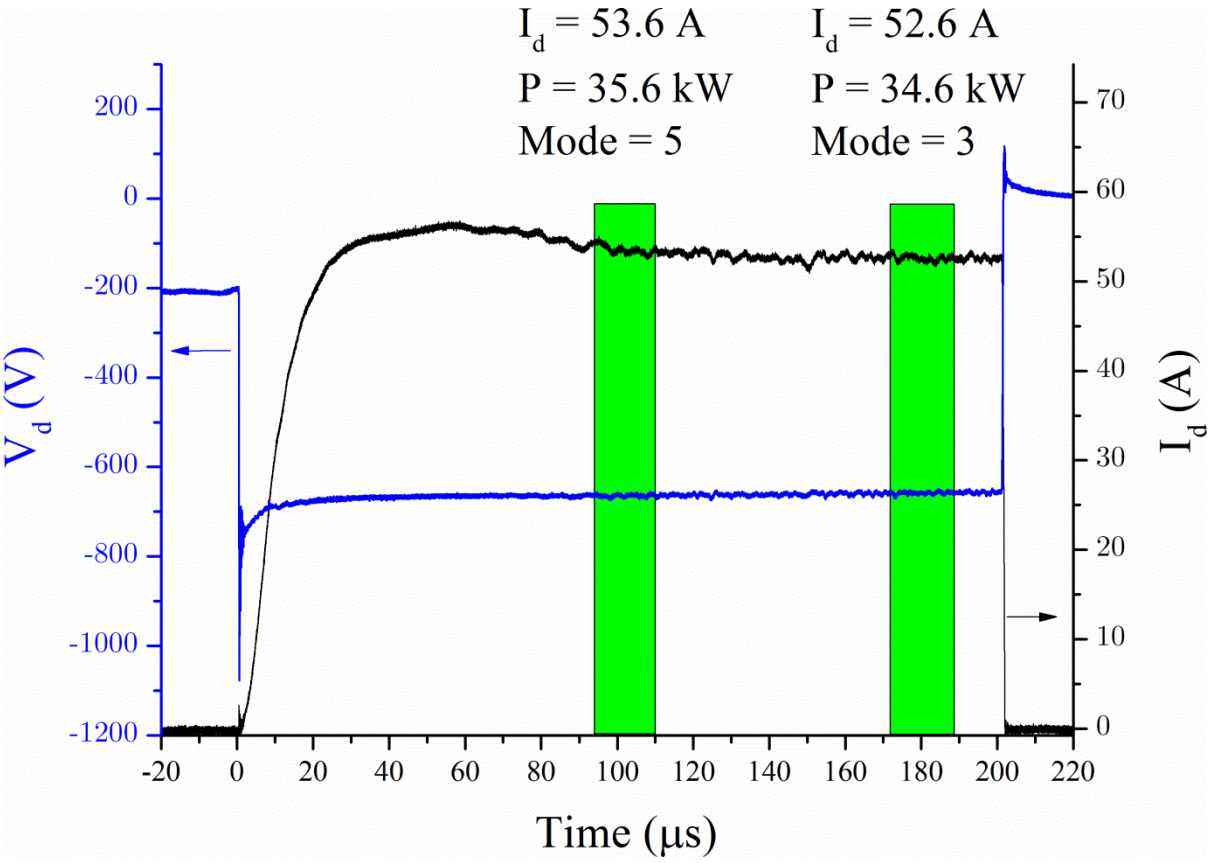

Figure 4).The discharge current and voltage time-traces for a 200 μs pulse. The operating pressure was 1 Pa for a pulse of energy of 6.8 J. Two selected periods are highlighted (by green rectangles) correspond to times with a mode number of m = 5 and m = 3. The average power and current during those periods is shown in the figure.

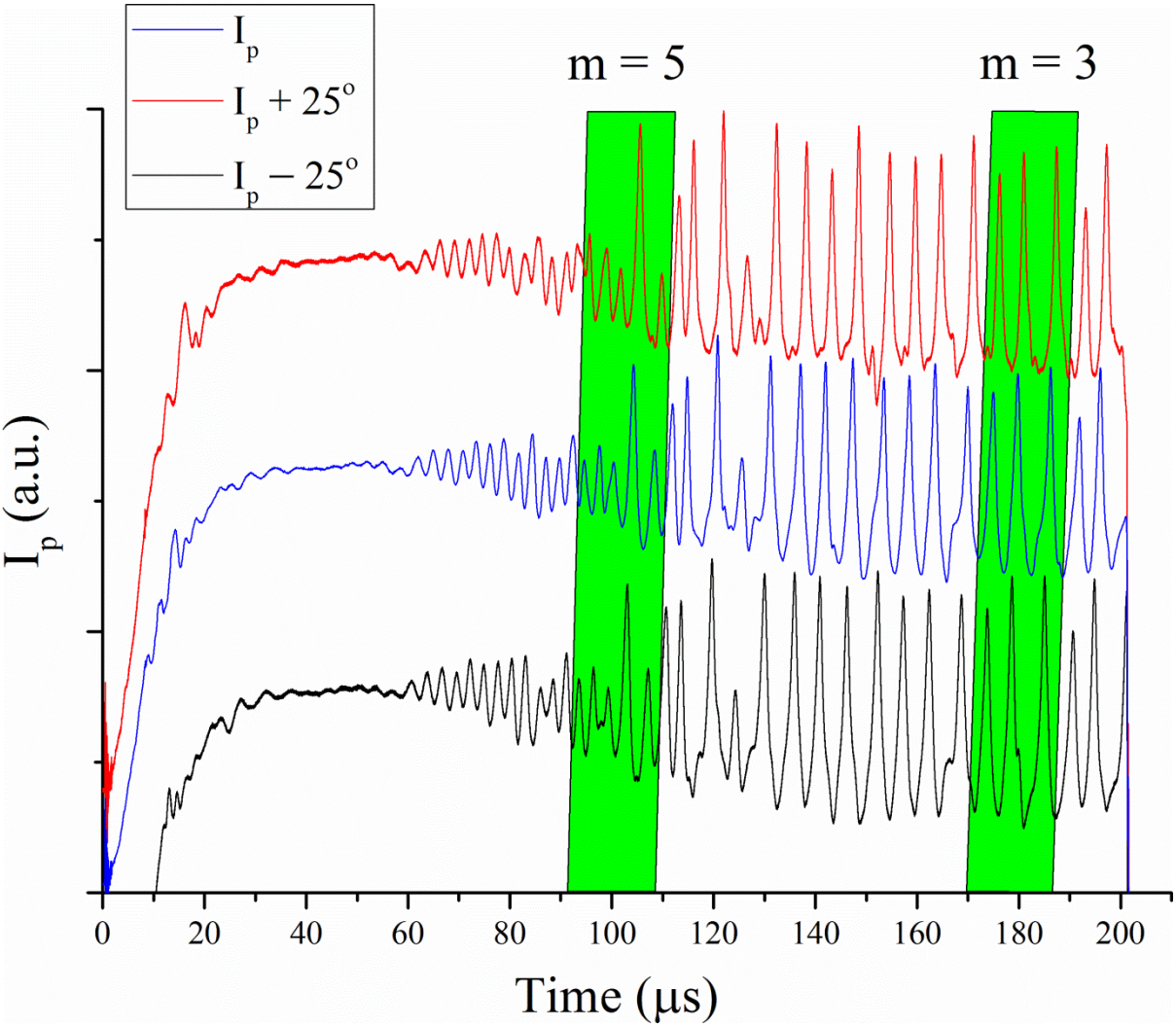

Figure 5) A plot of all three strip probe currents I_p, $I_{p+25}{}^{o}$ and $I_{p-25}{}^{o}$ during the HiPIMS pulse shown in figure 4. The highlighted periods correspond to times with a mode number of m = 5 and m = 3. The tilted parallelograms reveal the phase shifts in the signals between probes, used to calculate the spoke velocities. An arbitrary displacement in the strip probe current plots has been introduced to allow all three to be clearly seen.

3. Results and Discussion

In this study, we chose only one set of operating conditions to work at, namely an argon pressure of 1 Pa, a 200 μs plasma on-time, a 1 Hz frequency and a pulse energy of 6.8 J. This set of conditions was known to provide coherent spokes [12]. Figure 4 shows the discharge voltage V_d and current I_d time-traces over a period encompassing all of the pulse on-time. The average on-time target power density was 0.75 $kWcm^{-2}$. The vertical green rectangles

represent times when the spoke patterns show mode numbers of m = 5 and m = 3 respectively. From here on in, we chose to concentrate on these intervals, namely t = 94 to 110 μs and t = 172 to 189 μs into the pulse, where spokes are coherent and there is no merging or splitting events. The simultaneously recorded target currents I_p for the three embedded target strip probes are shown in figure 5. The widths of the green strips in the figures 4 and 5 represent a full spoke rotation period for the two modes. Clearly, strong oscillations in I_p can be seen which we attribute to the presence of coherent spokes as previously reported and discuss in length in [12] and confirmed by simultaneous 2D imaging in [15]. The phase shift in I_p between the azimuthally separated strip probes, as revealed in figure 5 by the tilt in the green parallelograms, allows the spoke velocities v_{sp} to be calculated at different times during the pulse. During the highlighted m = 5 period v_{sp} = 8.81 km s^{-1} while for m = 3 we have v_{sp} = 8.39 for km s^{-1}. The spokes rotate in the E x B direction. There is no discernible signature of spokes in the total discharge current I_d (see figure 4) as expected.

Figure 6 shows the time-traces for the triple and strip probe acquired parameters n_e, T_e, I_{isat}, I_p, V_f and plasma potential V_p over most of on-time of the chosen HiPIMS pulse. The time trace of I_p was taken from the central strip situated directly below the triple probe. The plasma potential V_p was estimated using V_f and T_e according to simple sheath theory [53] to be:

$$V_p = V_f + \frac{kT_e}{2e}\mathrm{Log}_e\left[\frac{m_i}{2\pi m_e}\right] + \frac{kT_e}{2} \qquad (5)$$

where m_e is the electron mass. Assuming m_i for argon ions, we have $V_p \sim V_f + 5kT_e/e$. The Log_e term in equation 5 is insensitive to m_i so our approximate expression for V_p is good even if niobium ions are the dominant species in the probe vicinity. There are strong and coherent oscillations in the measured quantities. This can be seen by calculating the mean ratio of the full peak-to-peak amplitudes of the oscillation to the minimum values in the troughs for each case. For the m = 5 interval, we have $\Delta n_e/n_e \sim 25$ %, $\Delta T_e/T_e \sim 36$ %, $\Delta I_{isat}/ Ii_{sat} \sim 42$ %, $\Delta V_f/V_f \sim 18$ %, $\Delta V_p/V_p \sim 120$ % and $\Delta I_p/I_p \sim 31$ %, while for the m = 3 mode interval these ratios are $\Delta n_e/n_e \sim 62$ %, $\Delta T_e/T_e \sim 51$ %, $\Delta I_{isat}/ I_{isat} \sim 42$ %, $\Delta V_f/V_f \sim 26$ %, $\Delta V_p/V_p \sim 190$ % and $\Delta I_p/I_p \sim 49$%. It is evident that these ratios are somewhat larger in the latter case than the former. This indicates that in our measurements at least stronger, better-

formed spokes exist at the lower mode number, more clearly delineated from the background. For increasing mode numbers the inter-spoke distances must reduce and it seems reasonable to think that there may be a smearing out of plasma parameter structures and a decrease in the local maxima relative to the background as spokes start to effectively overlap each other with close proximities. It has not been possible to obtain triple probe data in the off-time of the pulse, since the low plasma density conditions lead to larger overlapping sheaths at the probe tips and the conditions for validity of the method described in section 2.4 are not met.

Features in the I_p data are smooth and well defined since I_p signals are obtained directly at the target. These signals are robust as the strip probe area is large and it is also non-perturbing to the spokes. By contrast, the triple probe obtained values of T_e, n_e and V_p have been derived from time-traces in I_{isat} and V_f, themselves measured directly inside the active region of the spokes (where it is highly dynamical in nature), and so perturbing to the spokes. Nevertheless, time-traces in these plasma parameters, as shown in figure 6 are coherent and well-formed.

From the highlighted sections of the I_p time-traces in figure 6 we can see that as a spoke travels across the strip probe, the target current rises from a base level to a maximum and then falls again as it passes. Close inspection of the figure reveals however, that the leading edge of the spoke rises more slowly than trailing edge, consistent with previous observations made using the strip probe but with an aluminium target [12]. This slow rising and fast decreasing profile, which is characteristic of a wedged shaped spoke, is very clearly identified later in paper (in figure 9 which shows an expanded view of the m = 3 mode data). In addition, we see that the peaks in I_p are sharp while the troughs are rounded.

Inspection of I_p and I_{isat} in figure 6 shows that the peaks in ion current to the target occur during times of peak ion current to the triple probe, however the time-profiles of the later are very much broader. The minima in these quantities are concurrent and we infer that these quantities are essentially in-phase. By contrast, the peak values in T_e and n_e are not concurrent (there is a phase-shift) but do lie with the envelop defined by the board flat top of the I_{isat} profile as one would expect since I_{isat} ($\propto n_e T_e^{1/2}$) is a convolution of n_e and T_e. The time traces of the probe measured parameters also have somewhat inverted structures compared to I_p with sharp troughs and rounded peaks.

Despite the phase shifts, all the probe-determined parameters are coherent and correlated to modulations in I_p which gives us confidence that we are observing spokes directly or at least their immediate influence. In a recent article we showed that I_p matches well the distribution in optical intensities of the spokes as obtained with a fast camera [15].

Given I_p as our reference, we see that peaks in n_e are occurring towards the front of the spoke, while the highest values of T_e are seen at the rear, or even partially into the region between spokes. This appears as a phase shift between n_e and T_e of about 50^o; such phase shifts (and larger) between these parameters were also reported in a HiPIMS plasma using a triple probe but not attributed to spokes [40]. For the m = 3 mode the highest electron densities (up to n_e ~2.1 x 10^{19} m^{-3}) coincide with low electron temperatures (T_e ~2.1 eV), while peak values in T_e (~3.9 eV) are in regions of comparatively low electron density (n_e ~1.2 x 10^{19} m^{-3}) towards the rear of the spoke. Similar structures are seen with the m = 5 mode, however with a reduced magnitude in the parameter range.

The electron density time-traces reveal that at an elevated position, n_e rises quickly at the front of the spoke and decays more slowly towards the rear, in reverse to that seen in I_p (which is known to define the typical spoke shape). The n_e profiles in some spokes have something of a flattish top, particularly for m = 3.

The largest values in n_e and I_p are spatially separated (they appear towards the front and rear of the spoke respectively). Ions created at rest in the dense plasma region, some 15 mm above the target, will free-fall through the cathode pre-sheath and sheath to the target while the spoke itself and the following spokes are advancing around the racetrack.

The calculated V_p time-traces show that the maximum positive plasma potentials (up to + 9 V) occur at the rear of the spoke as defined by the I_p time-trace and are displaced from the leading n_e peaks. The minima in V_p (~ 0 V) are situated between spokes. In previous emissive probe studies in HiPIMS plasma [54], the time-averaged plasma potential V_p values in the near target pre-sheath were measured to be close to ground potential, or even a few 10's of volts more negative than ground. In those studies, the positive potentials associated with any spokes present in the discharge were not resolved.

In a detailed study using simultaneously emissive and single probes, large potential differences, up to 70 V, within spokes were observed in a low-power DC magnetron [11] with spokes rotating in the -E x B direction. The fastest rise in potential (from a negative value between spokes to a value close to ground) was seen at the leading edge of the spokes. In that article it was argued that the spatial distribution of the ion density within the spoke region should match well the spatial distribution of electron energies, but also the highest (most positive) plasma potentials. Here, we do not see such a coincidence of n_e and V_p. This may be due to the very different nature of our HiPIMS plasma compared to the very low-power (< 30 W) DC magnetron used in [11]. With high instantaneous powers (~35kW), strong rarefaction of the background argon gas may occur in our discharge leading to high concentrations of sputtered niobium atoms and ions (in multiple charge states) [14], [23], [55] within the dense plasma region. An increase in the number of energy loss in-elastic collisions between electrons and metal species would reduce the local electron temperature, where we measure the electron density to be at its highest. Since the triple probe measurements are made only at one height (15 mm) above the target, we do not have information on n_e and T_e at the point of maximum sputtering, i.e. where I_p is a maximum.

The strong correlation in the triple probe measurements of the plasma parameters at a height of 15 mm from the target and the I_p time-traces reassures us that we are indeed sampling the spokes, or at least a region of perturbed plasma, just above spokes but co-rotating with them. This region could contain electron flares, (tilted jets of electrons) which have been seen emanating from the top of spokes using slide-on views with a streak camera [21], [26]. These flares have elongations of up to 20 mm above the spokes with spokes themselves having typical heights of up to 5 mm.

In this study, the n_e time-traces (figure 6) do reveal some micro-oscillations (frequencies of ~ 5 x 10^6 Hz) during the peak (semi-plateaux) regions. This may just be instrumental noise, however since the oscillations seem less prevalent at times between spokes, it may indicate the presence of features in the plasma such as plasma flares (electron jets) emanating from the top of spokes [26] or oscillations in the azimuthal electric field driven by modified two-stream instabilities [56]. The lack of fidelity in the measurements does not allow us to draw any firm conclusions here. In terms of observing narrow-columned plasma flares, it does seem unlikely however that all three probe tips could see the same event simultaneously. In

the recent DC magnetron study of spoke potentials [11], the spoke structures were observed at heights well above 25 mm from the target, however no evidence of flares in the V_p data was presented.

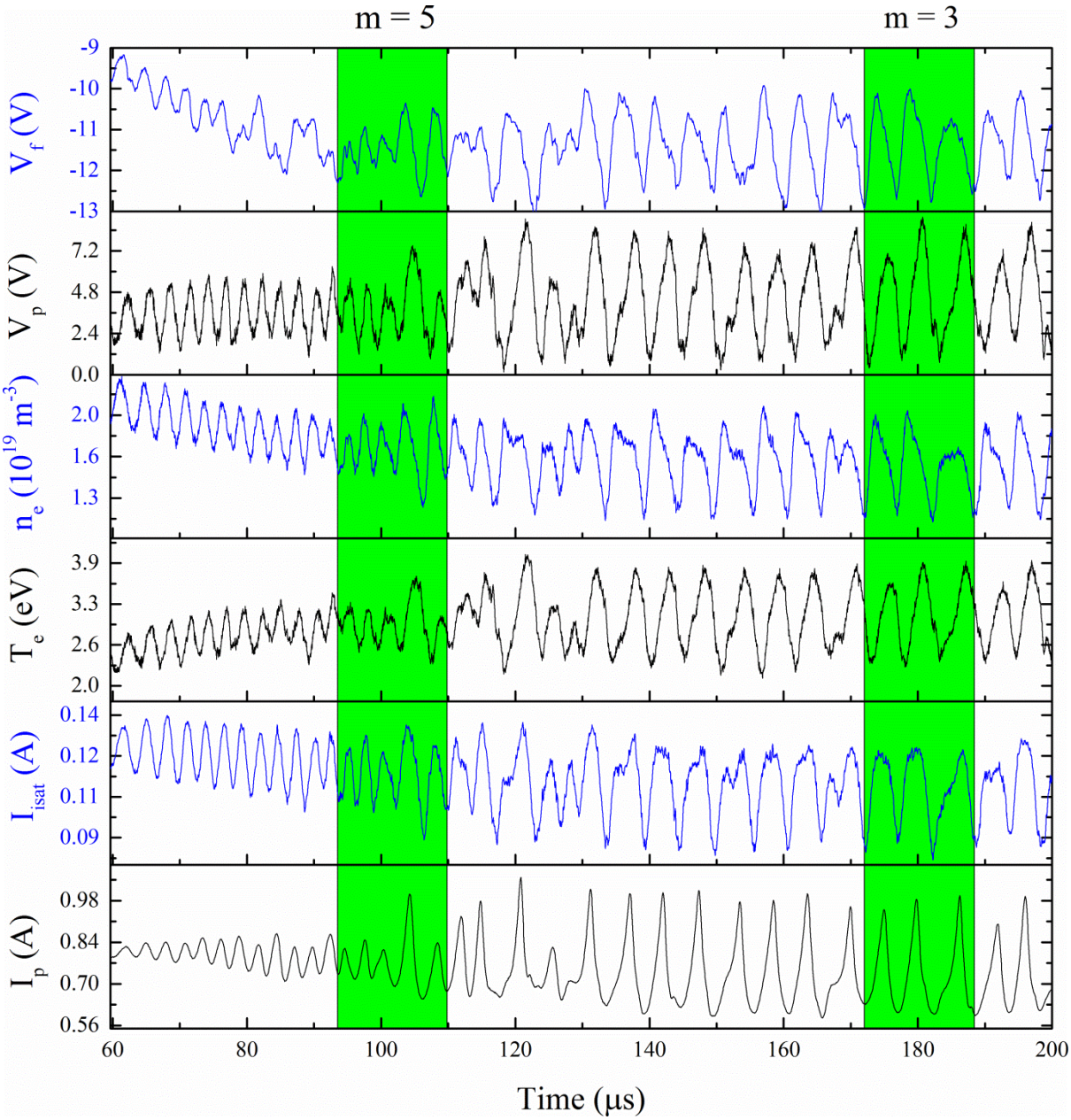

Figure 6. Time traces of strip probe current I_p, the triple probe measurements of ion saturation current I_{isat}, electron temperature T_e, electron density n_e, floating potential V_f and plasma potential V_p during a single HiPIMS pulse. The green rectangles indicate m = 5 and m = 3 modes respectively. The m = 3 interval data is shown in more detail later in section 3 (in figure 9) but re-plotted as a function of azimuthal angle.

The time-dependent data highlighted in figure 6 can be re-plotted as a function of azimuthal angle to produce a "snap-shot" image of the spoke plasma parameters which is pleasing to the eye and resembles typical 2-D ICCD optical images of spokes. In this way, phase shifts between the quantities become very apparent. To do this however, we must make an assumption about the radial plasma parameter profiles since the data was collected at only one radial position (of width 2.26 mm).

The triple probe determined parameters of T_e, n_e and V_p and the target probe current density J_p (ratio of I_p and the strip probe wetting area 50 mm^2) are chosen to be represented in this from for the stable m = 5 and m = 3 regions shown in figure 6.

We assume a complete period of spoke rotation has a rigid body structure and transform time t to the azimuthal coordinate θ, using $\theta = \omega t$, where $\omega = 2\pi/T$ is the spoke angular frequency. T is the spoke period. To provide radial coordinates (missing in the data) we assume the chosen parameters have a Gaussian radial distribution that peaks at the positions of the triple probe, namely at r_0 (= 21.5 mm), so for instance for the electron temperature T_e we have:

$$T_e(r,\theta) = T_e(\theta) exp - \left[\frac{r-r_0}{L}\right]^2$$

where L (= 10 mm) is an assumed mean radial width of the spokes (as used in [12]). The assumption of a Gaussian radial profile fits well observations from previous studies [57]. In the case of the strip probe current density $J_p(\theta)$, which is obtained from I_p over the narrow strip from the magnetron centre to the outer edge, we ensure that the integral of the constructed function $J_p(\theta, r)$ over the entire cathode gives the measured discharge current, namely:

$$\iint_{0,0}^{2\pi,R} J_p(\theta,r) r \, d\theta \, dr = A \iint_{0,0}^{2\pi,R} J_p(\theta) \, exp - \left[\frac{r-r_0}{L}\right]^2 r \, d\theta \, dr = I_d \, .$$

where A is a scaling constant. Performing the integral yields, in the particular cases chosen here, scaling constants of A = 1.69 of m = 3 and A = 1.57 for m = 5.

The resultant snap-shot images are shown in figures 7 and 8 for the m = 5 and m = 3 intervals respectively. Although of a partially assumed form they do provide realistic distributions,

somewhat similar to 2-D optical images of spokes. The wedge shape associated with spokes can be clearly seen in the target current data J_p, as previously observed using the strip probe method [12] and numerous optical studies, for example [15], [23]. One should bear in mind that the plasma parameter distributions shown refer only to a plane of height 15 mm above the target (with spatially averaged values over a 5 mm region defined by the tip lengths). For both mode cases (m = 5 and m = 3) the spoke as defined by their I_p footprint are evenly spaced.

To show better the phase relationship between all the measured parameters in the m = 3 interval, we have chosen to re-cast the time-dependent data in that section of figure 6 to be a function of the azimuthal coordinate θ. These plots are shown in figure 9 together with the reconstructed 2D images for V_p, $n_{e,}$ T_e and $J_{p.}$ Please note I_p in figure 6 has been converted to J_p. In this way, features in the 1-D data and the 2-D images, such as the peaks and troughs in the rotating structures, can be easily related to each other using the shown construction lines. In addition, to show better this phase relationship between the structure of intrinsic plasma parameters ($n_{e\,,}$ T_e and V_p), contour plots of n_e and T_e and n_i and V_p have been overlaid on the J_p distribution for the m = 3 case, see figures 10a and b respectively.

Only 3 contour lines are shown for the triple probe determined parameters, to avoid crowding the image. The spatial splitting between n_e and T_e is thrown into sharp relief (in figure 10a), with the intersection of these parameters coinciding with the peak in J_p, (and as can be seen in the raw data in figure 9 or in I_p if one refers back to the data in figure 6).

The ion current collected by the triple probe is governed by the Bohm criterion, with $J_{isat} \propto n_e T_e^{1/2}$ where n_e and T_e are the local values at a height of 15 mm above the target. By contrast the measured strip probe current I_p will have contributions from ions created at different heights in the spoke plasma, with a range of arrival times. If the high density leading edge seen at a height of 15 mm was present in a column all the way down to the foot of the spoke, then the slowly rising leading edge of I_p would not be observed, but instead a steep edge instead. Our observations therefore indicate that spokes may become denser with height at the leading edge.

There is however a correlation between the triple probe-measured current I_{isat} and the strip probe measured ion current I_p (or J_p) as shown in figures 6 (and 9), with peaks and troughs in both quantities being reasonably well aligned. The regions of high I_{isat} indicate positions at 15 mm height where the plasma is both relatively hot and dense (i.e. an overlap in T_e and n_e contours in figure 10a). It seems reasonable to assume that these conditions persist all the way down to the bottom of the spoke, so providing a peak in I_p measured on the target at about the same azimuthal location.

Similar displacements in n_e and V_p around the azimuth are seen in figure 10b. The most positive potentials are clearly evident at the rear of the spoke, where T_e is greatest. Using the data in figure 6 (and shown in more detail in figure 9) it is possible to determine the azimuthal electric field structure E_θ within the spokes. Inspection of V_p does show V_p rising more slowly at the front of the spoke and falling quickly towards the rear, implying the largest electric field E_θ are at the rear. The azimuthal electric field given as $E_\theta = dV_p/rd\theta = 1/v_{sp} \times dV_p/dt$ is calculated to be ~ 0.5×10^3 Vm^{-1} and ~1×10^3 Vm^{-1} at these positions respectively, somewhat similar in value to the low kVm^{-1} field strengths measured (with greater fidelity than our method) at a height of 15 mm above the target for spokes in a DC magnetron [11]. These regions of positive potential (the humps) evident at the rear of the spokes in figures 7, 8 and 10b will act to push positive ions created there out radially but also towards the leading and trailing edges of the spoke. Electrons, including those circling in the E x B direction, will be accelerated across these fields, heating the local electron population, leading to elevated T_e values. Such processes, associated with spoke potential hump double layers are discussed with clarity and detail in reference [11].

The wedge-shaped profile in the target current I_p and current density J_p seen in figures 6 and 9 respectively, with a slow build-up in the leading edge and a rapid decrease in the trailing edge, may be a consequence of this electron heating. Since the E x B drift speeds are greater than the spoke speeds, Hall drifting electrons must enter the spoke at the rear. Once heated in the spoke they continue their motion around the racetrack, losing energy through inelastic collisions with heavy species as they travel. The resultant tapered profile in J_p simply reflects the spatial distribution of the electron-energy dependent ion creation rate ahead of the spoke. For experiments in which spokes rotate in the –E x B direction, this tapered feature will be observed at the rear of the spoke [11].

Our triple probe measurements at a fixed location above the target reinforce the idea that spokes are an advancing region of intense ionization characterised by positive space potentials, relative to the surrounding regions. The triple probe detects locally a high density region at the front of the spoke well in advance of the build-up of ion current from the spoke to the target (i.e. the maximum in I_p lags the maximum in n_e).

Ions that constitute this target current I_p will travel a comparatively long distance from their origin in dense plasma (high up in the spoke structure) to the target. The typical transit time τ for ions (moving with say the ion acoustic speed) to travel down distance h from the dense plasma to the cathode target sheath edge is given as $\tau = h/(kT_e/m_i)^{1/2}$. For $kT_e/e \sim 2.5$ eV and h = 15 mm, such a transit time would be $\tau \sim 6$ μs (equivalent to an azimuthal rotation of $\theta = 134^o$), enough time for the spoke to have advanced ~48 mm around the racetrack. Therefore, ions arriving to the target from different heights (up to 15 mm) in the leading edge will be smeared out inside following spokes, contributing to their I_p signature and not the spoke they were created in.

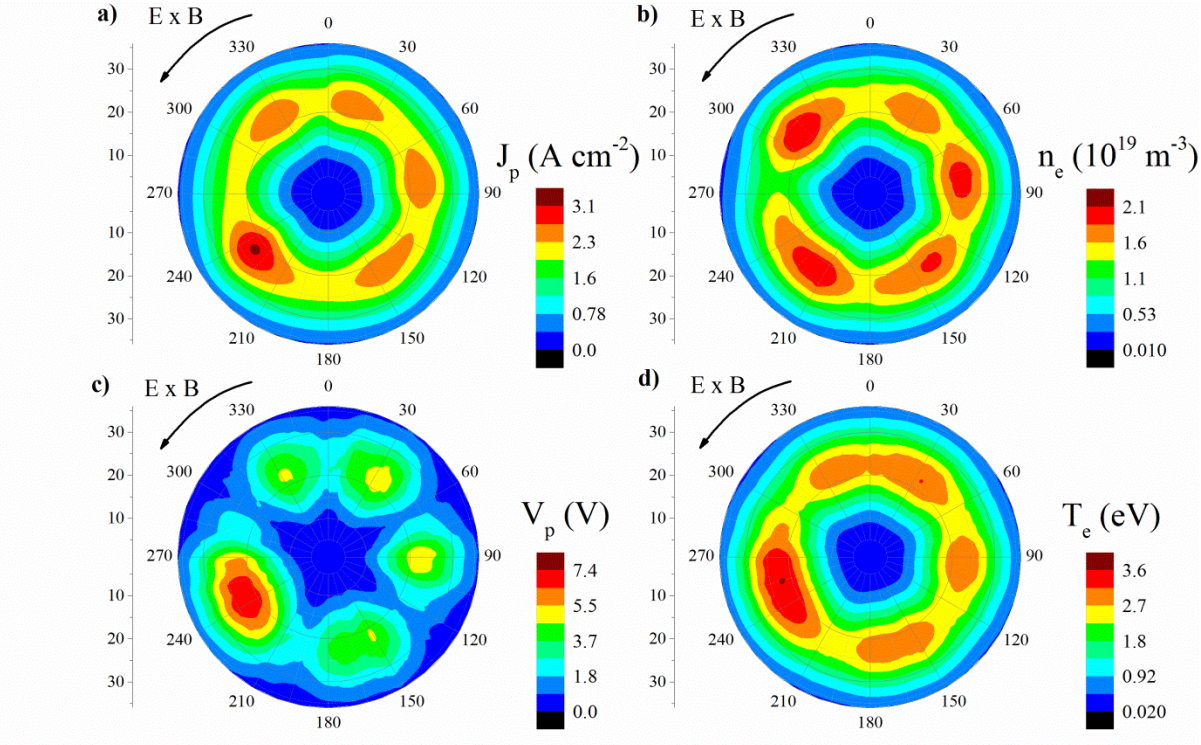

Figure 7. Constructed 2D images of a) the target ion current density J_p, b) the electron density n_e, c) the plasma potential V_p and d) the electron temperature T_e. The data was collected over one period during the chosen m = 5 interval (t = 94 to 110 μs). The triple probe measurements in b), c) and d) show the plasma parameters in the z = 15 mm plane above the target.

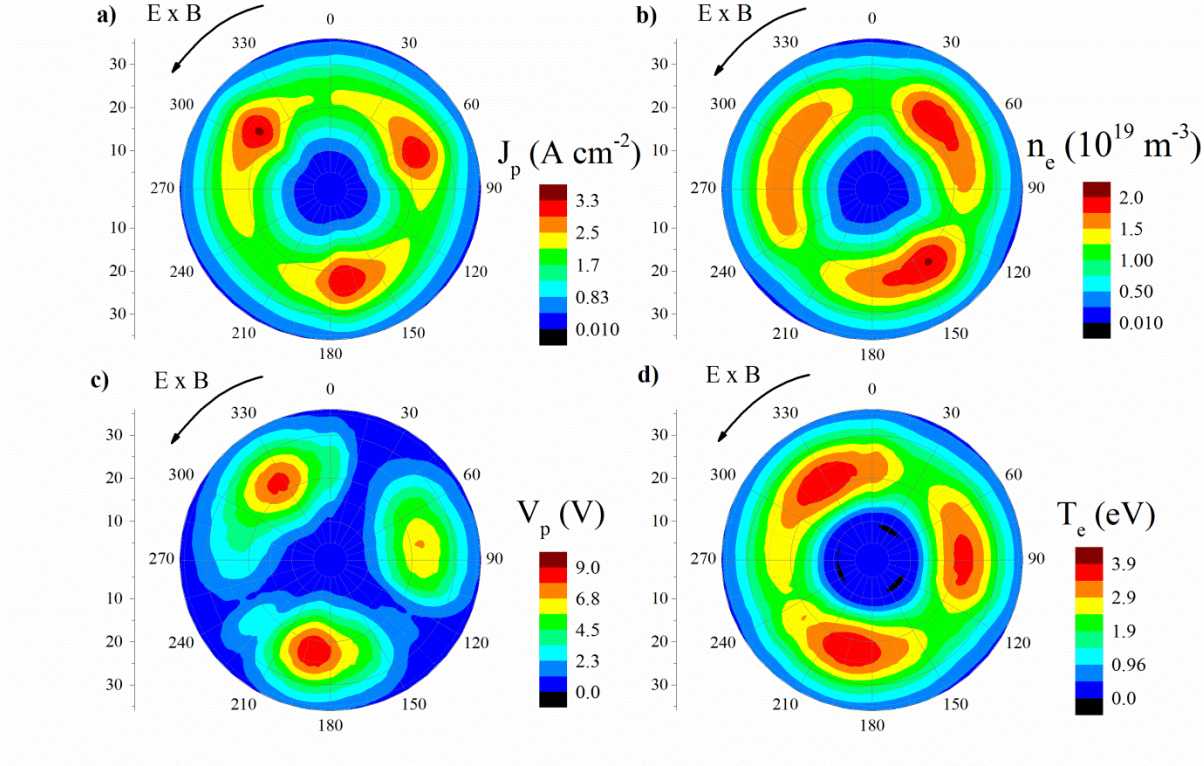

Figure 8. As figure 6 but for the m = 3 mode (t = 172 to 189 μs).

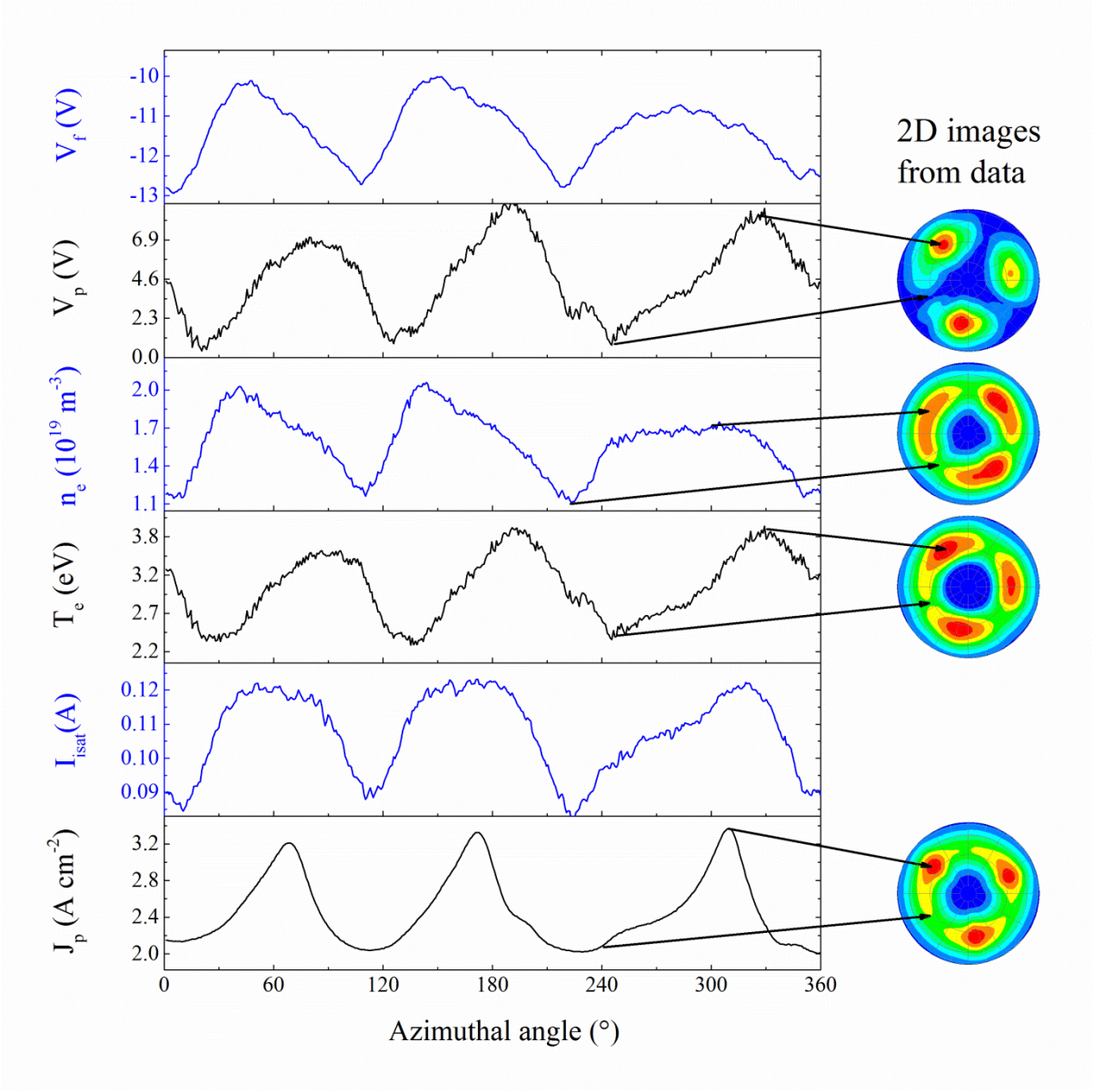

Figure 9. The strip probe current density at the centre of the racetrack J_p (derived from I_p) and the triple probe measurements of ion saturation current I_{isat}, temperature T_e, electron density n_e, floating V_f and plasma potential V_p plotted as a function of azimuthal angle as well as chosen 2-D images during the m = 3 interval. The plot is made from a transform of the data shown in figure 6.

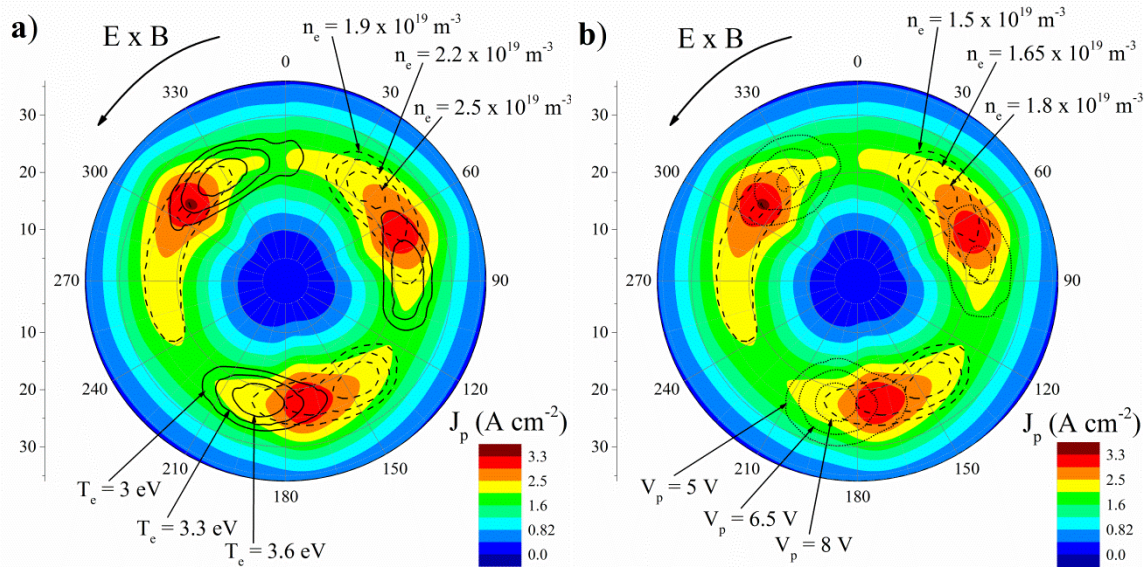

Figures 10 a) Three contour lines for the electron density n_e and temperature T_e overlaid on a colour map of the target current distribution J_p and b) three contour lines for n_e and the plasma potential V_p overlaid over the same colour map. The data is a re-plot for that shown in figure 8 for the chosen m = 3 mode interval of the HiPIMS pulse.

4. Conclusions

Using a combination of a triple probe and embedded target probes, the temporal evolution of the plasma parameters associated with rotating spokes in a HiPIMS plasma has been investigated. The electron density n_e, electron temperature T_e, plasma V_p and floating V_f potentials across a single cut plane 15 mm above the racetrack have been determined, a position where the triple probe intersects or is in close proximity to the spokes. The target probes show the spokes rotate in the E x B direction displaying coherent m = 5 and m = 3 modes within a single HiPIMS pulse.

With spoke shapes defined by their ion current density footprint J_p to the target, spokes were found to have higher electron densities and lower electron temperatures at their front ($n_e \sim 2.0 \times 10^{19}$ m^{-3}, $T_e \sim 2.1$ eV) but lower electron densities and higher electron temperatures at their rear ($n_e \sim 1 \times 10^{19}$ m^{-3}, $T_e \sim 3.9$ eV). Typically, the amplitude of the modulation in the n_e and T_e due to passing spokes was up to about 50 % of their mean values between spokes. A calculation of V_p based on V_f and T_e measurements show that here spokes have a positive potential hump of up to +9 V relative to the inter-spoke region. However these regions are spatially separated from the region of maximum n_e, with the potential humps towards the rear of the spoke. Azimuthal electric fields of 1kV/m are associated with these double layer structures.

From knowledge of the spoke velocity and mode number, time-traces of T_e, n_e, V_p and J_p have been transformed into functions of azimuthal angle allowing 2D spatial snap shot representations of the parameters to be made, assuming a radial profile. In this way we can see well that regions of maximum ion current to the target from individual spokes coincides with the overlap of high n_e and T_e regions measured above the target (at a height of 15 mm).

The triple probe measurements indicate that spokes have a complex structure with considerable electron densities (2×10^{19} m^{-3}) even at elevated positions above the target: Ions created in these regions will take about 6 μs to reach the target in which time the spoke will have advanced several cm's around the racetrack.

The usefulness of the triple probe method to diagnose spokes in HiPIMS plasmas is well demonstrated and more detailed studies including spatially resolved (radial and axial) measurements are planned.

Acknowledgements

F. Lockwood Estrin gratefully acknowledges the financial support from the EPSRC Centre for Doctoral Training in the Science and Technology of Fusion Energy (grant EP/L01663X/1).

References

[1] D. Lundin and K. Sarakinos, "An introduction to thin film processing using high-power impulse magnetron sputtering," *J. Mater. Res.*, vol. 27, no. 5, pp. 780–792, 2012.

[2] J. Bohlmark, J. Alami, C. Christou, A. P. Ehiasarian, and U. Helmersson, "Ionization of sputtered metals in high power pulsed magnetron sputtering," *J. Vac. Sci. Technol. A Vacuum, Surfaces, Film.*, vol. 23, p. 18, 2005.

[3] J. T. Gudmundsson, N. Brenning, D. Lundin, and U. Helmersson, "High power impulse magnetron sputtering discharge," *J. Vac. Sci. Technol. A Vacuum, Surfaces, Film.*, vol. 30, p. 30801, 2012.

[4] P. Poolcharuansin and J. W. Bradley, "Short- and long-term plasma phenomena in a HiPIMS discharge," *Plasma Sources Sci. Technol.*, vol. 19, no. 2, p. 25010, 2010.

[5] R. K. Waits, "Planar magnetron sputtering," *J. Vac. Sci. Technol.*, vol. 15, no. 2, pp. 179–187, 1978.

[6] A. Vetushka and J. W. Bradley, "The current-density distribution in a pulsed dc magnetron deposition discharge," *J. Phys. D. Appl. Phys.*, vol. 40, no. 7, pp. 2037–2044, 2007.

[7] N. Brenning and D. Lundin, "Alfvéns critical ionization velocity observed in high power impulse magnetron sputtering discharges," *Phys. Plasmas*, vol. 19, p. 93505, 2012.

[8] A. Hecimovic, C. Maszl, V. Schulz-von der Gathen, M. Böke, and A. von Keudell, "Spoke rotation reversal in magnetron discharges of aluminium, chromium and titanium," *Plasma Sources Sci. Technol.*, vol. 25, no. 3, p. 35001, 2016.

[9] A. V. Kozyrev, N. S. Sochugov, K. V. Oskomov, A. N. Zakharov, and A. N. Odivanova, "Optical studies of plasma inhomogeneities in a high-current pulsed magnetron discharge," *Plasma Phys. Reports*, vol. 37, no. 7, pp. 621–627, 2011.

[10] M. Panjan, S. Loquai, J. E. Klemberg-Sapieha, and L. Martinu, "Non-uniform plasma distribution in dc magnetron sputtering: origin, shape and structuring of spokes," *Plasma Sources Sci. Technol.*, vol. 24, no. 6, p. 65010, 2015.

[11] M. Panjan and A. Anders, "Plasma potential of a moving ionization zone in DC magnetron sputtering," *J. Appl. Phys.*, vol. 121, no. 6, p. 63302, 2017.

[12] P. Poolcharuansin, F. Lockwood Estrin, and J. W. Bradley, "The use of segmented cathodes to determine the spoke current density distribution in high power impulse magnetron sputtering plasmas," *J. Appl. Phys.*, vol. 117, no. 16, p. 163304, 2015.

[13] T. D. L. Arcos, V. Layes, Y. A. Gonzalvo, V. S. Der Gathen, a Hecimovic, and J. Winter, "Current–voltage characteristics and fast imaging of HPPMS plasmas: transition from self-organized to homogeneous plasma regimes," *J. Phys. D. Appl. Phys.*, vol. 46, p. 335201, 2013.

[14] A. Hecimovic, V. Schulz-von der Gathen, M. Böke, A. von Keudell, and J. Winter, "Spoke transitions in HiPIMS discharges," *Plasma Sources Sci. Technol.*, vol. 24, no. 4, p. 45005, 2015.

[15] P. Klein, F. Lockwood Estrin, J. Hnilica, P. Vašina, and J. W. Bradley, "Simultaneous electrical and optical study of spoke rotation, merging and splitting in HiPIMS plasma," *J. Phys. D Appl. Phys.*, vol. 50, p. 15209, 2017.

[16] C. L. Ellison, Y. Raitses, and N. J. Fisch, "Cross-field electron transport induced by a rotating spoke in a cylindrical Hall thruster," *Phys. Plasmas*, vol. 19, no. 1, 2012.

[17] P. B. Barber, D. A. Swift, and B. a Tozer, "The formation of rotating plasmas in a homopolar configuration," *J. Phys. D. Appl. Phys.*, vol. 5, no. 4, pp. 693–700, 2002.

[18] C. Maszl, W. Breilmann, J. Benedikt, and A. von Keudell, "Origin of the energetic ions at the substrate generated during high power pulsed magnetron sputtering of titanium," *J. Phys. D. Appl. Phys.*, vol. 47, p. 224002, 2014.

[19] M. Panjan, R. Franz, and A. Anders, "Asymmetric particle fluxes from drifting ionization zones in sputtering magnetrons," *Plasma Sources Sci. Technol.*, vol. 23, no. 2, p. 25007, 2014.

[20] R. Franz, C. Clavero, J. Kolbeck, and A. Anders, "Influence of ionisation zone motion in high power impulse magnetron sputtering on angular ion flux and NbOx film growth," *Plasma Sources Sci. Technol.*, vol. 25, no. 11pp, p. 15022, 2015.

[21] A. Anders, P. Ni, and A. Rauch, "Drifting localization of ionization runaway: Unraveling the nature of anomalous transport in high power impulse magnetron sputtering," *J. Appl. Phys.*, vol. 111, no. 5, p. 53304, 2012.

[22] A. Hecimovic, N. Britun, S. Konstantinidis, and R. Snyders, "Sputtering process in the presence of plasma self-organization," *Appl. Phys. Lett.*, vol. 110, no. 1, p. 14103, 2017.

[23] A. Hecimovic, M. Böke, and J. Winter, "The characteristic shape of emission profiles of plasma spokes in HiPIMS: the role of secondary electrons," *J. Phys. D. Appl. Phys.*, vol. 47, no. 10, p. 102003, 2014.

[24] T. D. L. Arcos, R. Schröder, Y. A. Gonzalvo, V. S. Der Gathen, and J. Winter, "Description of HiPIMS plasma regimes in terms of composition, spoke formation and

deposition rate," *Plasma Sources Sci. Technol.*, vol. 23, no. 5, p. 54008, 2014.

[25] A. P. Ehiasarian, A. Hecimovic, T. De Los Arcos, R. New, V. Schulz-Von Der Gathen, M. Bke, and J. Winter, "High power impulse magnetron sputtering discharges: Instabilities and plasma self-organization," *Appl. Phys. Lett.*, vol. 100, no. 11, p. 114101, 2012.

[26] P. A. Ni, C. Hornschuch, M. Panjan, and A. Anders, "Plasma flares in high power impulse magnetron sputtering," *Appl. Phys. Lett.*, vol. 101, no. 22, p. 224102, 2012.

[27] A. von Keudell, A. Hecimovic, and C. Maszl, "Control of High Power Pulsed Magnetron Discharge by Monitoring the Current Voltage Characteristics," *Contrib. to Plasma Phys.*, vol. 56, no. 10, pp. 918–926, 2016.

[28] W. Breilmann, C. Maszl, and A. von Keudell, "Fast charge exchange ions in high power impulse magnetron sputtering of titanium as probes for the electrical potential," *Plasma Sources Sci. Technol.*, vol. 26, no. 3, p. 35007, 2017.

[29] Y. Yang, X. Zhou, J. X. Liu, and A. Anders, "Evidence for breathing modes in direct current, pulsed, and high power impulse magnetron sputtering plasmas," *Appl. Phys. Lett.*, vol. 108, no. 3, p. 34101, 2016.

[30] G. J. Winter, A. Hecimovic, T. De los Arcos, M. Böke, and V. Schulz-von der Gathen, "Instabilities in high-power impulse magnetron plasmas: from stochasticity to periodicity," *J. Phys. D. Appl. Phys.*, vol. 46, no. 8, p. 84007, 2013.

[31] a Hecimovic, M. Böke, and J. Winter, "Plasma surface interaction enhanced instability in HiPIMS discharge," *31st ICPIG, July 2013, Granada, Spain*, no. 4, pp. 19–21, 2013.

[32] S. Spagnolo, M. Zuin, R. Cavazzana, E. Martines, A. Patelli, M. Spolaore, and M. Colasuonno, "Characterization of electromagnetic fluctuations in a HiPIMS plasma," *Plasma Sources Sci. Technol.*, vol. 25, p. 65016, 2016.

[33] M. Schubert, M. Endler, and H. Thomsen, "Spatiotemporal temperature fluctuation measurements by means of a fast swept Langmuir probe array," *Rev. Sci. Instrum.*, vol. 78, no. 5, p. 53505, 2007.

[34] S. L. Chen and T. Sekiguchi, "Instantaneous direct-display system of plasma parameters by means of triple probe," *J. Appl. Phys.*, vol. 36, no. 8, pp. 2363–2375, 1965.

[35] T. Ming, W. Zhang, J. Chang, J. Wang, G. Xu, S. Ding, N. Yan, X. Gao, and H. Guo, "Improvement of divertor triple probe system and its measurements under full graphite wall on EAST," *Fusion Eng. Des.*, vol. 84, no. 1, pp. 57–63, 2009.

[36] P. M. Bryant, S. A. Voronin, J. W. Bradley, and A. Vetushka, “Time-resolved triple probe investigations of a pulsed magnetron discharge,” *J. Appl. Phys.*, vol. 102, no. 4, p. 43302, 2007.

[37] J. Alami, J. T. Gudmundsson, J. Bohlmark, J. Birch, and U. Helmersson, “Plasma dynamics in a highly ionized pulsed magnetron discharge,” *Plasma Sources Sci. Technol.*, vol. 14, no. 3, pp. 525–531, 2005.

[38] H. Yu, L. Meng, M. M. Szott, J. T. Meister, T. S. Cho, and D. N. Ruzic, “Investigation and optimization of the magnetic field configuration in high-power impulse magnetron sputtering,” *Plasma Sources Sci. Technol.*, vol. 22, no. 4, p. 45012, 2013.

[39] L. Meng, H. Yu, M. M. Szott, J. T. Mclain, and D. N. Ruzic, “Downstream plasma transport and metal ionization in a high-powered pulsed-plasma magnetron,” *J. Appl. Phys.*, vol. 115, p. 223301, 2014.

[40] L. Meng, A. N. Cloud, S. Jung, and D. N. Ruzic, “Study of plasma dynamics in a modulated pulsed power magnetron discharge using a time-resolved Langmuir probe,” *J. Vac. Sci. Technol. A Vacuum, Surfaces, Film.*, vol. 29, no. 1, p. 11024, 2011.

[41] T. E. Sheridan, M. J. Goeckner, and J. Goree, “Observation of two-temperature electrons in a sputtering magnetron plasma,” *J. Vac. Sci. Technol. A Vacuum, Surfaces, Film.*, vol. 9, no. 3, pp. 688–690, 1991.

[42] S. H. Seo and H. Y. Chang, “Electron transport in the downstream region of planar unbalanced magnetron discharge,” *J. Appl. Phys.*, vol. 96, no. 3, pp. 1310–1317, 2004.

[43] H. Backer and J. W. Bradley, “Observations of the long-term plasma evolution in a pulsed dc magnetron discharge,” *Plasma Sources Sci. Technol.*, vol. 14, no. 3, pp. 419–431, 2005.

[44] S. Gallian, J. Trieschmann, T. Mussenbrock, R. P. Brinkmann, and W. N. G. Hitchon, “Analytic model of the energy distribution function for highly energetic electrons in magnetron plasmas,” *J. Appl. Phys.*, vol. 117, no. 2, p. 23305, 2015.

[45] J. W. Bradley and H. Amemiya, “Plasma Pre-Sheath in Low Pressure Discharges Containing Beam Electrons of Finite Temperature,” *J. Phys. Soc. Japan*, vol. 63, no. 9, pp. 3295–3302, 1994.

[46] P. Poolcharuansin, B. Liebig, and J. Bradley, “Plasma parameters in a pre-ionized HiPIMS discharge operating at low pressure,” *IEEE Trans. Plasma Sci.*, vol. 38, no. 11 P, pp. 3007–3015, 2010.

[47] N. A. Gatsonis, L. T. Byrne, J. C. Zwahlen, E. J. Pencil, and H. Kamhawi, “Current-mode triple and quadruple Langmuir probe methods with applications to flowing

pulsed plasmas," *IEEE Trans. Plasma Sci.*, vol. 32, no. 5, pp. 2118–2129, 2004.

[48] M. A. Lieberman and A. J. Lichtenberg, *Principles of Plasma Discharges and Materials Processing: Second Edition*. JOHN WILEY & SONS, INC, Hoboken, New Jersey, 2005.

[49] D. Diver, *A Plasma Formulary for Physics, Technology and Astrophysics*. Wiley-VCH Verlag Berlin, 2011.

[50] G. Franz, *Low Pressure Plasmas and Microstructuring Technology*. Springer-Verlag Berlin Heidelberg, 2009.

[51] A. Anders, "Localized heating of electrons in ionization zones: Going beyond the Penning-Thornton paradigm in magnetron sputtering," *Appl. Phys. Lett.*, vol. 105, p. 244104, 2014.

[52] C. Theiler, I. Furno, A. Kuenlin, P. Marmillod, and A. Fasoli, "Practical solutions for reliable triple probe measurements in magnetized plasmas," *Rev. Sci. Instrum.*, vol. 82, p. 13504, 2011.

[53] I. H. Hutchison, *Principles of Plasma Diagnostics*. Cambridge University Press, 1987.

[54] A. Mishra, P. J. Kelly, and J. W. Bradley, "The 2D plasma potential distribution in a HiPIMS discharge," *J. Phys. D. Appl. Phys.*, vol. 44, no. 42, p. 425201, 2011.

[55] N. Britun, S. Konstantinidis, and R. Snyders, "An Overview on Time-Resolved Optical Analysis of HiPIMS Discharge," *Plasma Process. Polym.*, vol. 12, no. 9, pp. 1010–1027, 2015.

[56] D. Lundin, U. Helmersson, S. Kirkpatrick, S. Rohde, and N. Brenning, "Anomalous electron transport in high power impulse magnetron sputtering," *Plasma Sources Sci. Technol.*, vol. 17, no. 2, p. 25007, 2008.

[57] G. Clarke, A. Mishra, P. J. Kelly, and J. W. Bradley, "Cathode current density distributions in high power impulse and direct current magnetron sputtering modes," *Plasma Process. Polym.*, vol. 6, pp. 548–553, 2009.